Collision spectroscopy of $Ar^{8+}+H_2$ at low velocities ($v<1$ a.u.)

S. Bliman
Université de Marne la Vallée, IFIS, 5, Boulevard Descartes, Champs sur Marne, 77454 Marne la Vallée Cedex 2, France

M. Cornille
DARC Observatoire de Paris, UPR 176 CNRS, 92195 Meudon Cedex, France

B. A. Huber and H. Lebius
Département de Recherche Fondamentale sur la Matière Condensée, SI2A, CEA-Grenoble, 17, rue des Martyrs, 38054 Grenoble Cedex 9, France

A. Langereis and J. Nordgren
Department of Physics, Uppsala University, Box 530, S7521 Uppsala, Sweden

R. Bruch
Physics Department, University of Nevada, Reno, Nevada 89577-0058
(Received 14 May 1999)

Single and double electron transfer have been studied for the collision system $Ar^{8+}+H_2$ at low velocities ($v<1$ a.u.). X-ray ultraviolet and Auger spectroscopies complemented by translational energy gain and time-of-flight spectroscopies reveal details on the transfer mechanisms: in contrast to the other two-electron target system (He target), a channel is opened where electron capture takes place with further dissociation of H_2^+. We consider the target fragment dynamics and discuss possible molecule dissociation mechanisms. [S1050-2947(99)02010-7]

PACS number(s): 32.30.−r, 32.80.Dz, 34.70.+e

I. INTRODUCTION

Determination of cross sections for ion-atom and ion-molecule collisions is of importance for different applications such as plasma modeling. It is essential to understand the excited-state population dynamics, because it relates directly to the radiative emission pattern of plasmas. In the case of single electron capture by ground-state ions, optical observations in the x-ray vacuum ultraviolet (XVUV) and visible regions provide high-accuracy data where Doppler shift and broadening of transitions are negligible. Beyond data taking, the use of intensity-calibrated spectrometers makes excitation cross-section estimates possible [1]. For metastable projectiles, single capture generally ends in the formation of ions in doubly excited states, frequently energetically above the first ionization limit. These states are basically of the same kind as those seen in plasmas, formed by dielectronic recombination, which have specific stabilization patterns. In plasmas, the optical decays termed satellite emissions are of great interest but the Auger decay is ignored and cannot be investigated *in situ*. In collision studies, when both decay channels are observed, theoretical estimates of energies, radiative transition probabilities, Auger transition probabilities, and fluorescence yields of extended sets of levels are needed for the purpose of identifications; beyond that, cross sections and rate coefficients can be determined [2].

Extensive studies of the system $Ar^{8+}+He$ have been performed. The detailed features were analyzed and are reasonably well understood [3]. Double capture by the metastable projectile ends in the triply core excited magnesiumlike Ar^{6+} ion, the stabilization of which has been shown to take place via two successive Auger steps: in the first one, the system decays to the intermediate continua $Ar^{7+}(2p^5 3l3l')$, the second one getting the ion to the only available continuum $Ar^{8+}(2p^6)\,{}^1S_0$ [4]. For the case at hand, $Ar^{8+}+H_2$, single capture is straightforward to identify in the spectrum, although in contrast to the He target, dissociation of H_2 may take place. In the case of double electron capture, Auger decays are more difficult to analyze because not much is known about the atomic features and thus theoretical calculations are required. Even though many studies were performed and published, which discuss cross-section measurements, many aspects are left nearly unexplained [5–10]. In some other papers involving H_2 as a target, no special attention was given to its molecular nature, focusing only on the double capture mechanisms [11–13].

In Sec. II, we present the experiments and the applied methods together with the experimental results. In Sec. III, the discussion outlines the collision cross sections and features single capture, single capture with target dissociation, and double capture. In Sec. IV, we discuss the collision mechanisms. The existence of the possible dissociation of H_2 opens channels not observable with atomic targets and we discuss a possible electric-field-induced process.

II. EXPERIMENTAL ARRANGEMENTS, METHODS, AND RESULTS

The collision system $Ar^{8+}+H_2$ has been studied with different experimental techniques: on the one hand, XVUV photon spectroscopy was applied to the observation of the decay following single and double capture (SC and DC) at an energy of 80 keV. On the other hand, the translational energy gain spectroscopy (TES) technique was used at ener-

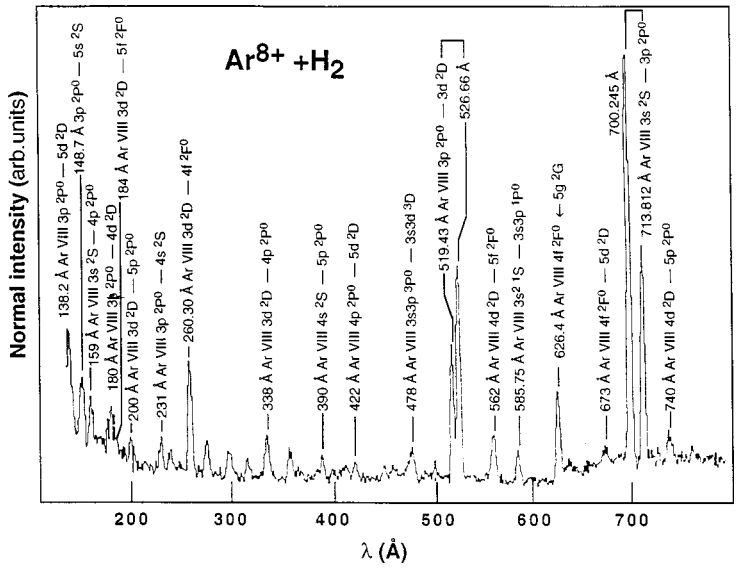

FIG. 1. XVUV absolute intensity calibrated spectrum observed in the 150–800-Å range for the collision $Ar^{8+}+H_2$, measured at 80 keV.

gies of 8 and 16 keV. This method, performed at zero degree and at small angles with respect to the incident ion-beam direction, gives access to the states populated in the collision. Auger spectra are also considered: these were recorded by other groups [14,15] under the same experimental conditions and are still open for analysis and discussion.

A. Optical spectroscopy in the vuv range

At a typical collision energy of 80 keV (2 keV/amu), the spectrum of the emitted radiation was recorded with the grazing incidence spectrometer described earlier [2]. Taking into account the intensity calibration of the device, the spectrum was reduced to the form shown in Fig. 1. In the short-wavelength region (100–160 Å), a second spectrometer [16] was used giving finer details; this spectrometer was not intensity calibrated on an absolute scale. However, in Fig. 2, the most intense lines are unambiguously attributed to the excitation of $Ar^{7+}(2p^6 5l)\,^2L$ and some weaker rays are originating from $Ar^{7+}(2p^6 6l)\,^2L$.

B. Translational energy gain and time-of-flight spectroscopies

The principle of the method and details on the experimental setup were described in previous publications [3,17]. A beam of Ar^{8+} ions is delivered by the ECR ion source of the A.I.M. facility. A double hemispherical electrostatic analyzer is used to narrow the energy and angle distributions of the primary beam [it yields an energy profile of 0.5 eV per charge full width at half maximum (FWHM)]. The beam interacts in the collision chamber with an effusive H_2 target. The collision chamber incorporates the first acceleration region of a Wiley-McLaren time-of-flight mass spectrometer, allowing for the measurement of the mass-to-charge ratio of the recoil target ions (molecules H_2^+ and fragments H^+). The secondary ions after SC and DC are detected at different scattering angles; they are analyzed with respect to their charge and kinetic energy with a second energy analyzer, which can be rotated around the collision chamber. From the analysis of the energy gain of the projectiles, the excitation energy and the populated states are determined.

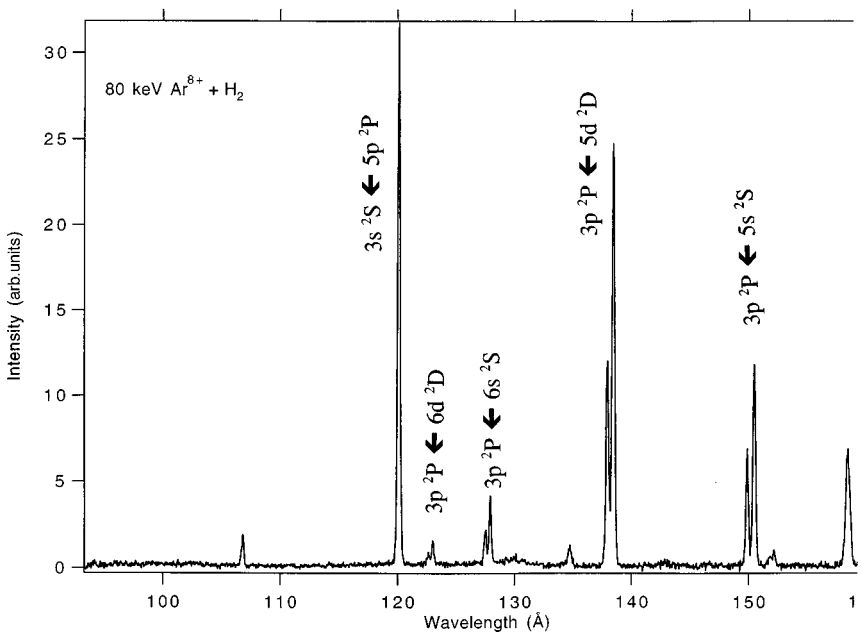

FIG. 2. XVUV spectrum observed in the wavelength interval 100–160 Å.

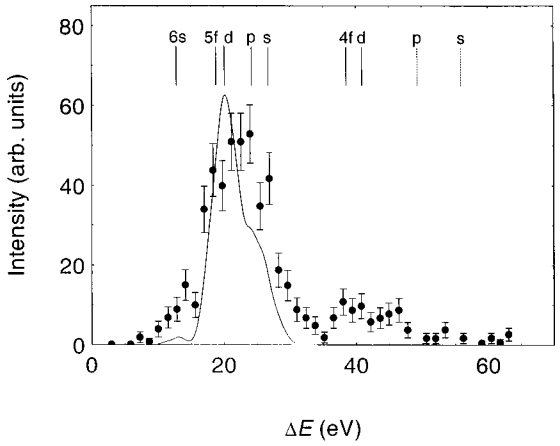

FIG. 3. Energy-gain spectrum of Ar^{7+} ions produced in Ar^{8+}/H_2 collisions at 8 keV; scattering angle 0°. The vertical lines indicate the position of capture into specific *nl* levels. The solid curve shows the result of a multichannel Landau-Zener calculation.

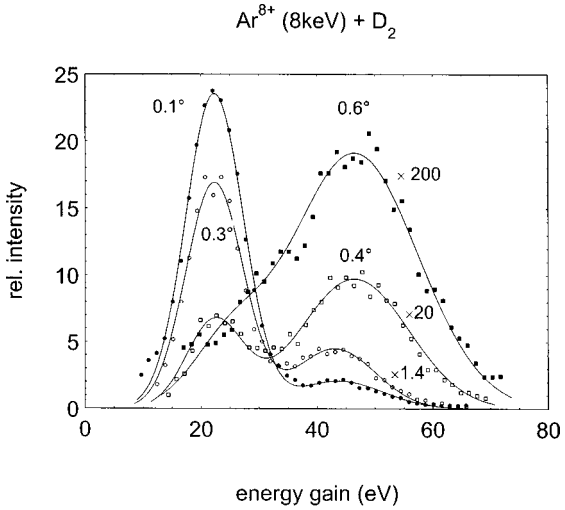

FIG. 4. Variation of the energy-gain spectrum with the scattering angle of the projectile. The different curves are normalized in intensity with respect to each other. Collision conditions as in Fig. 3.

Figure 3 shows a TES spectrum taken at $\delta=0°$ for the SC (Ar^{7+} ions). This spectrum is centered at an energy gain of about 20 eV; a weaker high-energy contribution occurs at about 40 eV. Neglecting excitation of the target, the peak at 20 eV may be attributed to SC of the transferred electron into $n=5$ states of the projectile, whereas the peak at 40 eV may be attributed to capture into $4f$ and $4d$ states. The full curve in Fig. 3 shows the result of a multichannel Landau-Zener calculation [18]. It represents the dominant contributions very well, favoring capture into the $5d$ level. In Fig. 4, the variation of the energy gain spectrum with the scattering angle of the projectile ($0°\leqslant\delta\leqslant 0.6°$) is shown for a collision energy of 8 keV. The different curves are normalized with respect to each other. Whereas for small angles capture into $n=5$ is dominant, larger energy gains become more prominent with larger scattering angles.

In order to test whether these contributions are due to dissociative or nondissociative processes, m/q spectra of the recoil ions have been measured in correlation with the kinetic energy gain of the projectiles of 20 and 45 eV, respectively. These spectra are shown in Fig. 5 for a scattering angle of 0.15°. At $\Delta E=20$ eV, the recoil spectrum consists only of H_2^+ ions, i.e., the capture process is nondissociative. At $\Delta E=45$ eV, the recoil spectrum shows dominantly H^+ ions; H_2^+ ions give only a small contribution. In this case, capture leads to the dissociation of the H_2 molecule. The H^+ ions form a double-peak structure, denoting ions with an initial kinetic energy which are emitted towards or away from the detector (ions emitted perpendicular to the extraction direction are not detected; this leads to the two distinct peaks). However, the question arises whether these H^+ ions stem from a dissociative single capture or whether they are due to transfer ionization processes. As electrons were not measured in coincidence, we used both the TES spectra from DC and the initial kinetic energy of the H^+ ions after single and double capture processes in order to further discuss this issue.

The TES spectrum for DC is shown in Fig. 6. The energy distribution is centered at about $\Delta E=50$ eV and corresponds to double capture into the $(4l,5l')$ configurations of Ar^{6+}. In Fig. 7, the TOF spectra of the H^+ peaks are shown, measured in coincidence with outgoing Ar^{7+} ions (SC and transfer ionization) and Ar^{6+} ions (DC). For all spectra, the time difference between both peaks is nearly the same (about 400 ns); their absolute position depends on the scattering angle of the projectile and whether the projectile is scattered slightly towards the recoil detector or into the opposite direction. This general shift of both peaks can be understood in terms of the kinematic energy transfer from the projectile to the target. Evaluating the time difference between the forward and the backward peak, one can deduce the amount of the initial kinetic energy due to dissociation. A time difference of 400 ns corresponds in the present case to a fragment energy of about 7.8 eV. The similarity of the energy gains and the fragment energies in the Ar^{6+} and Ar^{7+} case suggests that the major part of Ar^{7+} ions with energy gains of about 40–50 eV is due to transfer ionization. However, at least the presence of a low-energy peak, which has been measured only in correlation with Ar^{7+} ions and not with Ar^{6+} ions, seems to stand for dissociative single electron capture.

C. Auger spectrum

Finally, for the sake of completeness, in view of the analysis and interpretation, an Auger spectrum is shown in Fig. 8; it was taken under the same experimental conditions [14] as the vuv spectrum and was not fully analyzed and interpreted.

It appears that not much is known on the atomic features of the doubly excited levels Ar^{6+}** likely to be populated in the double transfer process. The spectrum was scanned and peak energies were precisely determined. The complete Auger spectrum comprises two parts.

(i) The low-energy part, extending from 0 to nearly 60 eV, relates to the DC by the ground-state projectile but in which are expected to be found some rays originating from the stabilization of the products from DC by the metastable ion. Only this low-energy part is considered here. In Fig. 8 we also show the reaction windows (dashed lines) for the DC with provision for the decay to the two available continua,

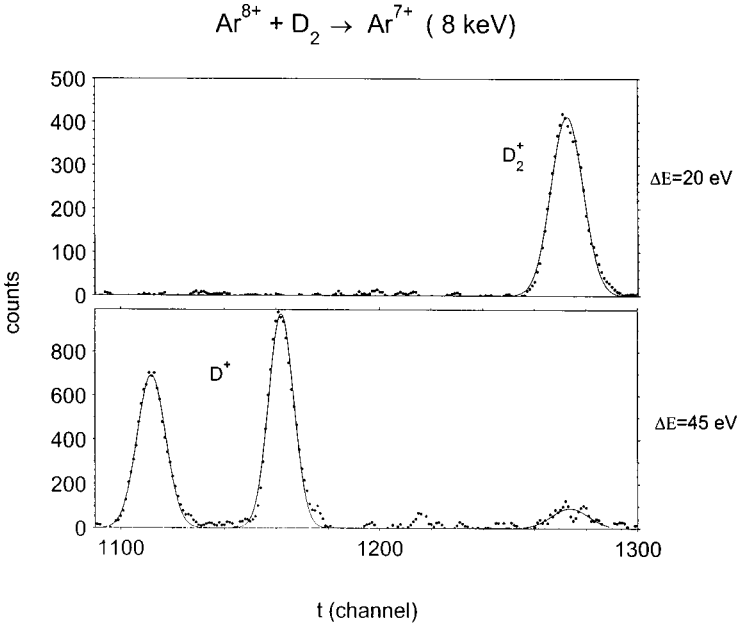

FIG. 5. Time-of-flight recoil spectrum measured in coincidence with projectiles (here Ar^{7+} ions) of a given energy gain. Upper part: $\Delta E = 20$ eV; lower part: $\Delta E = 45$ eV.

namely $Ar^{7+}(3p)$ and $Ar^{7+}(3d)$.

(ii) The high-energy part of this spectrum extends from 100 eV approximately up to nearly 265 eV and is attributed to the decay following SC and DC on the metastable ion (this will be treated in a separate paper).

III. CROSS SECTIONS AND COLLISION FEATURES

Even though H_2 is a two-electron target, its molecular nature opens more channels in charge-transfer collisions. We have to consider the following:

SC,

$$Ar^{8+} + H_2 \rightarrow Ar^{7+}(nl) + H_2{}^+. \quad (1)$$

SC and dissociation,

$$Ar^{8+} + H_2 \rightarrow Ar^{7+}(nl) + H^+ + H. \quad (2)$$

DC,

$$Ar^{8+} + H_2 \rightarrow Ar^{6+}{}^{**} + H^+ + H^+. \quad (3)$$

This last process may be followed by autoionization,

$$Ar^{6+}{}^{**} \rightarrow Ar^{7+} + e, \quad (4)$$

and/or photon emission,

$$Ar^{6+}{}^{**} \rightarrow Ar^{6+} + h\nu, \quad (5)$$

Dissociative SC (2) has to be considered, because its importance has been shown in experiments with other molecular targets and different multiply charged projectiles [19–21].

Beyond that, we know that in charge exchange collisions the projectile is left in the exit channel in excited states. For the purpose of evaluating the value of n (principal quantum number of the levels most likely to be populated), it is possible to use different models. Among them, two have been frequently used and agree quite well with the observations: the model proposed as early as 1981 by Mann *et al.* [22] gives the principal quantum number of the levels most likely to be populated in SC, whereas the extended classical overbarrier model [23,24] under certain assumptions may give the specific n values for multiple electron transfer. A difficult problem to solve is to estimate the orbital momentum l of those states which are populated with high probability. A scaling law has been proposed [25] that accounts for the kinematic conditions of the collision and of the nature of the target and projectile.

Keeping these considerations in mind, the following equations denote the major reaction channels.

SC,

$$Ar^{8+} + H_2 \rightarrow Ar^{7+}(5l)\,{}^2L_J + H_2{}^+. \quad (1')$$

SC+dissociation,

$$Ar^{8+} + H_2 \rightarrow Ar^{7+}(4l)\,{}^2L_J + H^+ + H(n=2), \quad (2')$$

$$Ar^{8+} + H_2 \rightarrow Ar^{7+}(5l)\,{}^2L_J + H^+ + H(n=1), \quad (2'')$$

while DC should end in

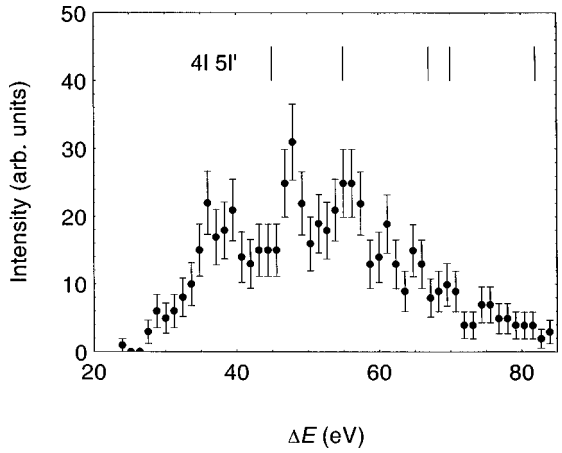

FIG. 6. Energy gain of Ar^{6+} ions produced by DC in Ar^{8+}/H_2 collisions. Collision energy: 8 keV; scattering angle: 0°.

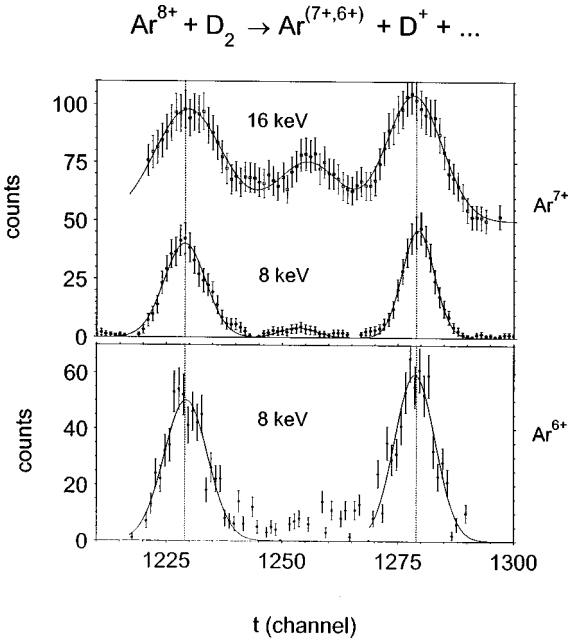

FIG. 7. Time-of-flight distribution of the H^+ fragments measured in coincidence with Ar^{7+} ions (upper curves, $\Delta E=45$ eV at two collision energies) and Ar^{6+} ions (lower part) after Ar^{8+}/H_2 collisions (the time scale has been slightly shifted for the different curves in order to superimpose the different peaks).

$$Ar^{8+}+H_2\rightarrow Ar^{6+}(4l,5l')+H^+ +H^+. \qquad (3')$$

The following set of orbital moments is most likely to be populated: SC $(1')$: $l=1,2$; SC+dissociation $(2')$: $l=0,1$; $(2'')$: $l=0,1,2$; DC $(3')$: $l=1,2$ and $l'=1,2$.

With this identification, it is possible to estimate cross sections at least for SC. For DC, first we will give the results of calculations performed to obtain the atomic features of $Ar^{6+}(4l,5l')$, so far not known.

A. VUV spectroscopy and cross-section estimates for SC and photon-stabilized DC

Most previous observations and cross-section determinations have been based on the measurement of the intensity of Ar^{7+} ions at the exit of the collision cell [5–10]. With the consideration of Eqs. (1), (2), and (4), it is not possible to discriminate the origin of these ions. However, the optical approach allows, under the condition that the spectrometer is intensity calibrated, for the determination of the cross sections [3]. The method consists of measuring the emission cross section σ_{em} for each individual transition for directly populated levels, when cascade contributions can be neglected. Correcting this quantity by the branching ratio [26], we get the excitation cross section of the upper level of the transition.

For the case at hand, the spectra show a very weak cascade population originating from $n=6$ to 5 (see Fig. 2). Therefore, the cross sections for the excitation of $n=5$ in Ar^{7+} are estimated to be

$$\sigma_{5s}=\sigma_{em}(5s\rightarrow 3p)/0.57=1.4\times 10^{-15}\ \text{cm}^2,$$

$$\sigma_{5p}=\sigma_{em}(5p\rightarrow 4s)/0.12=1.2\times 10^{-15}\ \text{cm}^2,$$

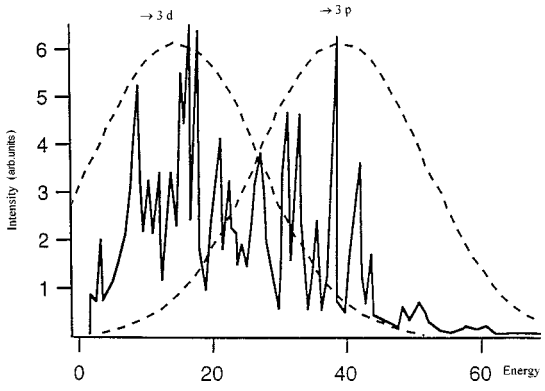

FIG. 8. Auger spectrum after DC in Ar^{8+}/H_2 at 80 keV. The spectrum has been scanned to ease line identifications. The dashed lines are the reaction window positions for Auger decays to the $3d$ continuum (low energy) and to the $3p$ continuum (higher energy).

$$\sigma_{5d}=\sigma_{em}(5d\rightarrow 3p)/0.85=1.4\times 10^{-15}\ \text{cm}^2,$$

$$\sigma_{5f}=\sigma_{em}(5f\rightarrow 4d)/0.30=0.46\times 10^{-15}\ \text{cm}^2,$$

$$\sigma_{5g}=\sigma_{em}(5g\rightarrow 4f)/0.99=0.71\times 10^{-15}\ \text{cm}^2,$$

This gives a total capture cross section into $Ar^{7+}(n=5)$ of about $5.2\times 10^{-15}\,\text{cm}^2$.

Comparing the different line intensities, it appears that the transitions originating from the $n=4$ substates have not only a cascade feeding from $n=5$ but also a direct feed $(2')$. Under these conditions, we determine a direct capture cross section into $4l$. The cascade feed from $5l'$ has to be deduced. Finally, we obtain

$$\sigma_{4s}=\sigma_{em}(4s\rightarrow 3p)-0.12\times\sigma_{5p};$$

this last factor is the emission cross section for the cascade feed of $4s$ from $5p$. Accordingly, we get for the other substates of $n=4$ the following emission cross sections:

$$\sigma_{4p}=\{\sigma_{em}(4p\rightarrow 3s)-0.43\times\sigma_{5s}-0.15\times\sigma_{5d}\}/0.57,$$

$$\sigma_{4d}=\{\sigma_{em}(4d\rightarrow 3p)-0.25\times\sigma_{5p}-0.32\times\sigma_{5f}\}/0.91,$$

$$\sigma_{4f}=\sigma_{em}(4f\rightarrow 3d)-\sigma_{5g}.$$

At 2 keV/amu, we obtain $\sigma_{4s}=2.9\times 10^{-16}$ cm^2, $\sigma_{4p}=7\times 10^{-16}$ cm^2, $\sigma_{4d}=0.7\times 10^{-16}$ cm^2, and $\sigma_{4f}=1\times 10^{-16}$ cm^2, yielding a total cross section for single electron capture into Ar^{7+} $(n=4)$ [process as proposed in Eq. $(2')$] of $\sigma_4=1.2\times 10^{-15}\,\text{cm}^2$. The uncertainty of these cross sections is of the order of 30% and, as was explained in Ref. [3], is basically due to the absolute calibration accuracy of the spectrometer.

Summing up, we obtain the total SC cross section, $\sigma_{SC}=6.3\times 10^{-15}\,\text{cm}^2$. It should be noted that this cross section is a factor of 3 larger than the value obtained with He as a target [3]. Accounting for the uncertainty, this value has the same magnitude as predicted by our scaling law [27], which gives in this case $8.5\times 10^{-15}\,\text{cm}^2$ with an error of the order 20%.

The true DC cross section, in the sense that both captured electrons remain on the projectile, ending after radiative cas-

cades in the ground state $Ar^{6+}(3s^2)\,^1S_0$ and in the lowest metastable state $Ar^{6+}(3s3p)\,^3P_J^0$, is determined by considering the end transitions:

$$3s3p\,^1P_1 \rightarrow 3s^2\,^1S_0,$$

$$3s3d\,^3D \rightarrow 3s3p\,^3P_0 \quad \text{and} \quad 3s4p\,^1P_1 \rightarrow 3s^2\,^1S_0.$$

From this, we may write

$$\sigma_{DC} = \sigma_{em}(2p^6 3s3p\,^1P_1^0 \rightarrow 3s^2\,^1S_0) + \sigma_{em}(2p^6 3s4p\,^1P_1^0 \rightarrow 3s^2\,^1S_0) + \sigma_{em}(2p^6 3s3d\,^3D \rightarrow 3s3p\,^3P).$$

Since the autoionizing DC does not interfere with the process of Eq. (1) in the sense that the available continua are the $Ar^{7+}(2p^6 3l)$ states, which are not directly populated and not considered for the SC cross section, we can obtain the DC cross section as the ratio of the sum of the intensities of the transitions contributing to the true DC to the sum of the intensities of the transitions contributing to the SC cross section. This gives $\sigma_{DC} = 1.0 \times 10^{-15}\,cm^2$, not accounting for the part of DC that stabilizes via Auger decay.

B. Auger spectrum

The first step in the analysis of the low-energy part of the spectrum shown in Fig. 8 consists in the calculation of the atomic features of the states expected to be populated, which are not known so far; we need to know the $Ar^{6+}(4l5l')^{1,3}L$ configurations.

We use the calculation method presented earlier [4]. We calculated all $2p^6 3ln'l'$ levels above the first ionization limit of $2p^6 3s^2$ and all the $2p^6 4l4l'$ configurations. We took into account the coupling and mixing between $2p^6 3dnl$ and $2p^6 4l4l'$. The results of the calculations performed for $Ar^{6+}(2p^6 4l5l')$, limited to $l = 0,1$ and $l' = 0,1$, are given in Table I. The table contains the energy of each level, given in eV with respect to its ground state, the sum of all transition probabilities ΣA_r, the sum of all Auger probabilities ΣA_a, and the corresponding total fluorescence yield defined as

$$\omega_T = \Sigma A_r / (\Sigma A_r + \Sigma A_a).$$

For some levels we give, in Table II, optical transition wavelengths when the fluorescence yield is significant. It should be kept in mind that the corresponding low intensity transitions might not be individually visible because of the low population of each directly populated level at the time of the DC. But, given the instrument sensitivity and since the cascade process contributes in the population increase of the intermediate and final levels (funnel type feed of the cascade termination), it is thus possible to observe the final transitions as pointed above. To facilitate the inspection of the Auger decays and to evaluate approximately the energy gains, the complete level scheme relevant to SC and DC is shown in Fig. 9. For this representation, the relevant quantities needed for H_2 (ionization potential, dissociation energy, and second ionization potential) were taken from [28] and [29]. From these values, it is possible to assign the energetic limits to the Auger series as they appear in the spectrum and relate them to the energy-gain spectrum as shown in Fig. 8. In Table III, we give the Auger electron energies for the different series $4l\ nl'$ decaying to the different available continua. Given the instrumental resolution, it is possible to make some assignments which show clearly that double cap-

TABLE I. Calculated atomic data of important Ar^{6+} $(4l,5l')$levels Column 1, level designation; column 2, energy from ground state (in eV); column 3, sum of all transition probabilities; column 4, sum of Auger probabilities; column 5 total fluorescence yield (see text).

Level	Energy (eV)/ ground state	$\Sigma A_r\,(s^{-1})$	$\Sigma A_a\,(s^{-1})$	ω_T
$4s5s\,^3S_1$	156.76	9.08[+09]	2.86[+12]	3.16[−3]
$4s5s\,^1S_0$	157.72	6.74[+09]	6.18[+13]	1.09[−4]
$4s5p\,^1P_1$	160.04	9.82[+09]	3.05[+13]	3.22[−4]
$4s5p\,^3P_0$	160.27			
$4s5p\,^3P_1$	160.28	6.7[+09]	1.16[+11]	5.46[−2]
$4s5p\,^3P_2$	160.31	6.7[+09]	1.15[+08]	9.83[−1]
$4p5s\,^3P_0$	163.98			
$4p5s\,^3P_1$	164.01	5.58[+09]	2.55[+11]	2.14[−2]
$4p5s\,^3P_2$	164.08	5.54[+09]	1.33[+10]	2.94[−1]
$4p5s\,^1P_1$				6.76[−5]
$4p5p\,^1P_1$	166.16	8.85[+09]	2.42[+12]	3.65[−3]
$4p5p\,^3D_1$	166.53	8.12[+09]	3.84[+12]	2.11[−3]
$4p5p\,^3D_2$	166.58	8.11[+09]	3.96[+12]	2.05[−3]
$4p5p\,^3D_3$	166.65	8.12[+09]	3.81[+12]	2.13[−3]
$4p5p\,^3P_0$	167.18	9.64[+09]	8.69[+13]	1.11[−4]
$4p5p\,^3P_1$	167.21	9.62[+09]	8.66[+13]	1.11[−4]
$4p5p\,^3P_2$	167.25	9.63[+09]	8.73[+13]	1.10[−4]
$4p5p\,^3S_1$	167.56	7.74[+09]	5.45[+12]	1.48[−3]
$4p5p\,^1D_2$	167.97	8.56[+09]	1.25[+14]	6.84[−5]
$4p5p\,^1S_0$	169.67	1.07[+10]	2.39[+14]	4.49[−5]

TABLE II. Most important optical transitions including levels with high fluorescence yields.

Upper Level	Lower level	ω_T	$\Sigma A_1\,(s^{-1})$	λ (Å)
$4s5p\,^3P_1$	$3s^2\,^1S_0$	5.46[−2]	6.71[+9]	77.35
	$3s4s\,^3S_1$			126.31
	$3s4s\,^1S_0$			128.91
	$3s4d\,^3D_1$			149.18
	$3s4d\,^3D_2$			149.19
	$3s4d\,^1D_2$			150.0
$4s5p\,^3P_2$	$3s4s\,^3S_1$	9.83[−1]	6.7[+9]	126.28
	$3s4d\,^3D_1$			149.15
	$3s4d\,^3D_2$			149.17
$4p5s\,^3P_1$	$3s^2\,^1S_0$	2.14[−2]	5.58[+9]	75.60
	$3s4s\,^3S_1$			121.68
	$3s4s\,^1S_0$			124.10
	$3s4d\,^3D_1$			142.77
	$3s4d\,^3D_2$			142.78
$4s5s\,^3P_2$	$3s4s\,^3S_1$	2.94[−1]	5.54[+9]	121.60
	$3s4s\,^3D_1$			142.66
	$3s4d\,^3D_2$			142.67
	$3s4d\,^3D_3$			142.69

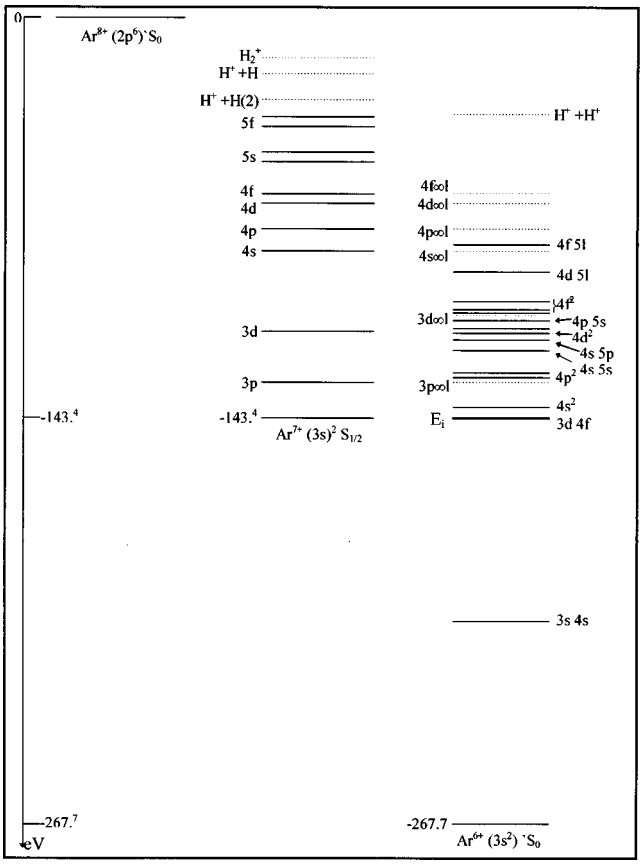

FIG. 9. Energy-level diagram showing the entrance channel (left column), the SC channel (center), and the DC channel (right column). The dashed lines indicate the different ionization energies from the entrance channel.

ture goes mostly into $4l\ 5l'$, pointing towards the lower angular momentum values. Even though it is currently accepted that these doubly excited states should decay to the nearest continua, the observations do not strictly confirm that statement. Some of these assignments are shown in Table IV. They are based on the determination of the reaction window as suggested by Mack [14] (use was made of the theory as proposed by Niehaus [24]) and on the estimate of the energy necessary to reach the system $H^+ + H^+$. It should be noted that there is a great number of low-intensity peaks, which cannot be assigned: these are probably due to the first of two Auger steps following the double capture by the metastable projectile $Ar^{8+}(2p^5 3s)\ ^3P$ [4] and will be studied in a separate paper with the XVUV spectrum. If we account for the autoionizing double-capture cross section as measured and given earlier ($\sigma_{ADO} = 1.9 \times 10^{-15}$ cm^2) [14,15], the total double-capture cross section is about 2.8×10^{-15} cm^2. This value is nearly 50% of the total single-capture cross section. In this collision the total fluorescence yield for DC is thus $\omega_T = 36\%$.

C. TES and TOF analysis of recoil ions

In Fig. 3, the peak at 20 eV corresponds to capture of the transferred electron into the $n=5$ states of the projectile (excluding target excitation), whereas the peak at 45 eV is the contribution to the capture into $n=4$ states and to the transfer ionization process. As already discussed before, coincidence measurements with the recoil ions have shown that at $\Delta E = 20$ eV, the recoil spectrum consists only of H_2^+ ions, i.e., the capture process is nondissociative. At $\Delta E = 45$ eV, the recoil spectrum exhibits mainly H^+ ions, i.e., the capture process has led to the dissociation of the molecule, either by single capture or transfer ionization.

TABLE III. Calculated Auger decay rates and electron energies for the decay to different available continua.

Level	Energy to $3s$ (eV)	Energy to $3p$ (eV)	Energy to $3d$ (eV)
$2p^6 4s^2\ ^{1,3}S$	23.1	17.5	
$4s5s$	32.7	15.2	
$4s5p$	35.7–40	18.2–23.5	
$4s\infty 1$	71.4	54	30
$2p^6 4p^2$ *S, P, D*	36.3–37	15.5–16.8	
$4p5s$	40	23.5	
$4p5p$	42	24.5	
$4p\infty l$	78	60.5	37
$2p^6 4d^2$ *D, F, G*	52.5–54	17.5–17.7	
$4d5l$	62	44.5	19
$4d\infty l$	86.5	69	45.3
$2p^6 4f^2$ *S, D, G*	59.5–63.8	17.7–17.8	2.5
$4f5l$	72	54.5	31
$4f\infty l$	89	74.5	47

Does the internuclear distance of the H_2 molecule change during the electron-capture process or not? Assuming Franck-Condon transitions for DC (no change of the internuclear distance), we expect kinetic energies of the fragment ions of the order of 9.7 eV, which is larger than the measured value of (7.8 ± 0.5) eV. The measured kinetic energy would translate into an internuclear distance of $1.7a_0$, about 24% larger than the equilibrium distance of $1.4a_0$ of the neutral molecule. This finding is in agreement with results published by the Kansas group [30], who concluded that only at much higher projectile velocities does the internuclear distance approach the Franck-Condon limit. Our value is in between their measured value of $2.25a_0$ for Ar^{5+} ions with 1 keV kinetic energy and the Franck-Condon limit. In this case, the E field carried in the interaction by the Ar^{5+} ion is weaker than in our case.

In the case of single-electron capture, different dissociative molecular potentials can be populated, leading to kinetic energies of the fragment ions in the range of 5–9 eV. Therefore, it is more difficult to conclude on the importance of non-Franck-Condon transitions. However, the TOF spectra shown in the upper part of Fig. 7 clearly demonstrate the presence of low-energy fragments, visible between the forward and the backward peak. These contributions increase with increasing projectile energy and scattering angle. According to Wood and Olson [31], the energy transferred in the collision and the dissociation energy might approximately be equal for certain orientations of the H_2 molecule. One fragment can stay at rest while the other one receives the total energy. As our detection system favors certain collision geometries (internuclear axes perpendicular to the ion beam), this effect might be more pronounced in the case of single-electron-capture processes.

TABLE IV. Auger transition assignments.

Level	Decay to $3d$ (eV)	Amplitude (a.u.)	Decay to $3p$ (eV)	Amplitude (a.u)	Decay to $3s$ (eV)	Amplitude (a.u.)
$4s5s$			15.3	4.45	31.5	1.62
$4s5p$			19.5	2.4	34.7	1.40
$4s\infty l$	29.8	0.6	53.7	0.14	72.9	0.06
$4p5s$			22.2	3.26	40.3	1.65
$4p5p$	3.1	2.02	26.1–27.5	3.2–3.85	42.7	0.7
$4p\infty l$	36.14	0.57	60.67	0.23		
$4d5l$	20.8–21.3	4.14–1.84	43.6	1.72		

IV. DISCUSSION

In view of the experimental results presented above, we can now discuss the following fundamental questions: is the dissociation taking place in the entrance channel of the collision or in the exit channel? Is the dissociation induced by the electric field and/or kinematically induced? In other words, is the transfer taking place from atomic hydrogen (as a result of $H_2 \rightarrow H+H$) or is electron transfer taking place from the molecule leaving H_2^+ or H_2^{2+}, which then dissociate?

In the experimental conditions, it is important to derive on the basis of the classical Coulomb law the order of magnitude of the electric field brought in by the projectile. At a distance of $4a_0$ between target and ion, the field is of the order of 7.3×10^8 V/cm (which corresponds to 0.2–0.3 a.u.). Moreover, we note, that if we consider the time of flight of the projectile necessary to pass the distance from 12 to 4 a.u. from the target, the molecule will feel a space and time field variation of the order of 1.5×10^{25} V/ms. It seems that the prevailing conditions compare with the conditions created in femtosecond laser pulses interacting with molecules, where the field intensity is high and the interaction time is long (compared to the collision time), giving an overall time-space variation for the electric field slightly larger than in the collision (1.5×10^{26} V/ms). But in contrast to the laser case, the interaction takes place in the presence of a continuously increasing electric field, which does not imply electromagnetic interaction. In the case of the laser, about 17 cycles of the laser radiation take place [32], thus allowing for photon exchanges and promotion up along the excitation levels ladder.

Given these remarks, we note that with a Landau-Zener potential curve crossing approach, the most probable single-electron transfer should take place at distances between the molecule and the Ar ion of the order of 7–8 a.u. This is reflected in Fig. 3, showing the counting rate versus the energy gain (solid curve: multichannel Landau-Zener calculation). From this, we would conclude that the dissociation would proceed while the ion gets closer to H_2^+, which then dissociates into $H^+ + H$. This is facilitated because the electric field has, in flight, distorted the molecular ion by a high-intensity Stark effect. We have also to consider the characteristic times in the actual experimental conditions: for this we have the time-ordering sequence:

$$t_{\text{collision}} < t_{\text{molecule vibration}} < t_{\text{observation}}$$

In these conditions, the importance of vibrational excitation of the molecule cannot be judged. Summing up, an electron is transferred first, then the dissociation process is supported by an E-field interaction distorting the molecule; this would possibly couple one potential curve of the molecular ion with the ion dissociation curve ([24], and references therein). Kinetic energy transferred during the collision can contribute to breaking the residual H_2^+ ion.

The photon spectra as analyzed give further credit to the possibility of a non-Franck-Condon dissociation, given the high value of the capture cross section into the $n=4$ manifold, pointing to the $4s$ and $4p$ states of Ar^{7+}. In [31], it is underlined that at increasing collision velocities toward values closer to 1 a.u., the dissociation process would deviate more and more from a Franck-Condon transition. This is what the spectroscopic observations seem to indicate, since referring to Fig. 9, all the quantities for the ionization dissociation and second ionization potential of H_2 and H_2^+ were taken as non-Franck-Condon values [28].

V. CONCLUSION

We have determined the cross sections of SC and DC for the system $Ar^{8+}+H_2$. They are relatively large and agree with the experimental scaling laws. The importance of the non-Franck-Condon dissociation has been underlined and is probably of primary importance. Since, in contrast to the femtosecond laser interaction with molecules, there is no photon exchange but a high-intensity continuously increasing electric field felt by the molecule; the strong field could modify the internuclear distance of the H atoms and thus facilitate the dissociation of the molecule. Further developments should involve the observation of the photon emission by the fragments of the molecules and also the use of ions with higher charges where the non-Franck-Condon dissociation is expected to become even more important.

ACKNOWLEDGMENTS

The optical (Fig. 1), Auger, and TES and TOF spectra have been measured at the Accélérateur d'Ions Multichargés, a facility of CEA-Grenoble. We would like to thank F. Gustavo for preparing the ion beam. The extreme VUV spectrum calculation was taken at the University of Nevada, Reno.

[1] R. Hoekstra, in *The Physics of Electronic and Atomic Collisions (XIX ICPEAC)*, edited by L. J. Dubé, J. B. A. Mitchell, J. W. McConkey, and C. E. Brion, AIP Conf. Proc. No. 360 (AIP, Woodbury, NY, 1996), p. 547.
[2] S. Bliman, M. Cornille, and K. Katsonis, Phys. Rev. A **50**, 3134 (1994).
[3] S. Bliman, M. G. Suraud, D. Hitz, B. A. Huber, H. Lebius, M. Cornille, J. E. Rubensson, J. Nordgren, and E. J. Knystautas, Phys. Rev. A **46**, 1321 (1992).
[4] S. Bliman, M. Cornille, B. A. Huber, and J-F Wyart, Phys. Rev. A **56**, 4683 (1997).
[5] S. Bliman, J. Aubert, R. Geller, B. Jacquot, and D. van Houtte, Phys. Rev. A **23**, 1703 (1981).
[6] J. P. Giese, C. L. Cocke, W. Waggoner, L. N. Tunnell, and S. L. Varghese, Phys. Rev. A **34**, 3770 (1986).
[7] M. Druetta, S. Martin, T. Bouchama, C. Harel, and H. Jouin, Phys. Rev. A **36**, 3071 (1987).
[8] P. Boduch, M. Chantepie, D. Hennecart, X. Husson, H. Kucal, D. Lecler, and I. Lesteven-Vaisse, J. Phys. B **22**, L377 (1989).
[9] J. Vancura, V. J. Marchetti, J. J. Perotti, and V. O. Kostrun, Phys. Rev. A **47**, 3758 (1993).
[10] S. Kravis *et al.*, Phys. Rev. A **52**, 1206 (1995).
[11] F. W. Meyer, C. C. Havener, R. A. Phaneuf, J. K. Swenson, S. M. Shafroth, and N. Stolterfoht, Nucl. Instrum. Methods Phys. Res. B **24/25**, 106 (1987).
[12] A. Bordenave-Montesquieu, P. Benoit-Cattin, M. Boudjema, A. Gleizes, and S. Dousson, Nucl. Instrum. Methods Phys. Res. B **23**, 941 (1987).
[13] M. Barat, M. N. Gaboriaud, L. Guillemot, H. Laurent, and S. Andriamonje, J. Phys. B **20**, 5771 (1987).
[14] M. Mack, Ph.D. thesis, University of Utrecht, The Netherlands (1987).
[15] M. Boudjema, Ph.D. thesis, Université d'Alger, Algeria (1990).
[16] J. Nordgren and R. Nyholm, Nucl. Instrum. Methods Phys. Res. A **246**, 314 (1986).
[17] H. Lebius and B. A. Huber, Z. Phys. D **21**, S271 (1991).
[18] H. Lebius, H. R. Koslowski, and B. A. Huber, Z. Phys. D **11**, 53 (1989).
[19] J. M. Hodgkinson, T. K. McLaughlin, R. W. McCullough, J. Geddes, and H. B. Gilbody, J. Phys. B **28**, L393 (1995).
[20] A. Remscheid, B. A. Huber, M. Pykavyj, V. Staemmler, and K. Wiesemann, J. Phys. B **29**, 515 (1996).
[21] F. Krok, Yu. Tolstikhina, H. A. Sakaue, I. Yamada, K. Hosaka, M. Kimura, N. Nakamura, S. Ohtani, and H. Tawara, Phys. Rev. A **56**, 4692 (1997).
[22] R. Mann, F. Folkmann, and H. F. Beyer, J. Phys. B **14**, 1161 (1981).
[23] A. Barany, G. Astner, H. Cederquist, H. Danared, S. Huldt, P. Hvelplund, A. Johnson, H. Knudsen, L. Liljeby, and K. G. Rensfelt, Nucl. Instrum. Methods Phys. Res. B **9**, 397 (1985).
[24] A. Niehaus, J. Phys. B **19**, 2925 (1986).
[25] R. Hutton, D. Schneider, and M. H. Prior, Phys. Rev. A **44**, 243 (1991).
[26] A. Lindgard and S. E. Nielsen, At. Data Nucl. Data Tables **19**, 533 (1977).
[27] S. Bliman, M. Bonnefoy, J. J. Bonnet, S. Dousson, A. Fleury, D. Hitz, and B. Jacquot, Phys. Scr. **T3**, 63 (1983).
[28] T. Odagiri, N. Uemara, K. Koyama, M. Ukai, N. Kouchi, and Y. Hatano, J. Phys. B **29**, 1829 (1996).
[29] C. J. Latimer, in *Abstracts of Contributed Papers, ICPEAC XVII, Brisbane, Australia*, edited by I. E. McCarthy, W. R. MacGillivray, and M. C. Standage (Hilger, Bristol, 1991) (detection of both H^+ fragments in coincidence).
[30] J. P. Giese, C. L. Cocke, W. T. Waggoner, J. O. K. Pedersen, E. Y. Kamber, and L. N. Tunnell, Phys. Rev. A **38**, 4494 (1988).
[31] C. J. Wood and R. E. Olson, Phys. Rev. A **59**, 1317 (1999).
[32] R. C. Constantinescu, S. Hunsche, H. B. van Linden van den Heuvell, H. G. Muller, C. Leblanc, and F. Salin, Phys. Rev. A **58**, 4637 (1998).